LIFELINE
EMERGENCY and SAFETY

Research Article

Bridge damage detection using PCA-DWT with limited sensors

Xiaojie Zheng[1,3], Honghong Li[4], Zhenhua Nie[1,✉], Hongwei Ma[2]

Cite this article: Zheng X J, Li H H, Nie Z H, et al. *Lifeline Emergency and Safety* 2026, **1**: 9660010. https://doi.org/10.26599/LLES.2025.9660010

ABSTRACT: Traditional bridge detection methods require a large number of sensors, which restricts the application in practical engineering. In order to reduce the cost of the health monitoring system and improve the accuracy of bridge damage detection, a bridge damage detection method based on principal component analysis and discrete wavelet transform is proposed. This method performs principal component analysis on the displacement under moving load and obtains the first principal component composed of dynamic component and modal shape. The first principal component is separated by the low-pass filter to receive the dynamic component of the first mode. Then the dynamic component is analyzed by the discrete wavelet transform to obtain the wavelet coefficient. Then the wavelet coefficient is used to reconstruct the signal. Finally, damage index is defined by using the reconstructed signal to detect the damage. When the structure is damaged, the damage index peaks at the damage location. In order to verify the effectiveness of the method, a beam bridge is simulated and a steel beam bridge is tested in the laboratory. Both simulation and experimental results show the proposed method can accurately identify the damage location in various scenarios with limited sensors.

KEYWORDS: Structural damage detection; limited sensors; principal component analysis; discrete wavelet transform

1 Introduction

Structural deterioration or damage can arise from changes in load characteristics, environmental impacts and random effects[1]. Damage detection serves as a fundamental role in the health monitoring, which mainly contributing to the extension of the lifespan for the structure.

Damage detection can be divided into three primary methods: the time domain method[2,3], the frequency domain method[4,5] and the time-frequency domain method[6]. Frequency-domain methods relying on modal parameters[7] face practical limitations in engineering applications due to their dependence on dense sensor arrays for high-resolution modal shape acquisition. This challenge has motivated the development of time-frequency domain techniques[8-10], with wavelet transform (WT) emerging as a representative solution. The Discrete Wavelet Transform (DWT), as a discrete implementation of WT, enables precise damage detection through bridge response analysis[11]. Its ability to capture damage-induced variations under moving loads has stimulated numerous investigations. Zhu et al.[12] leveraged the mid-span response induced by moving loads on a beam bridge to extract wavelet coefficients, which were regarded as a damage index for crack detection. Similarly, Khorram et al.[13] adopted the wavelet coefficients to detect the damage in the bridge. Nguyen and Tran[14] detected the damage of the bridge which employed DWT to analyze the response and accurately localize the damage. However, these conventional wavelet methods demonstrate limited sensitivity to minor damage. To enhance detection capability, researchers have integrated DWT with the Teager Energy Operator (TEO) to amplify localized signal features. Sha et al.[15] employed data fusion and TEO based on DWT to enhance the sensitivity to detect small damage. Xin et al.[16] combined TEO with DWT to process the mode curvature, and this method can identify small damage. However, these methods above are vulnerable to noise and external excitations, making them prone to false judgement particularly in the presence of abrupt changes or fluctuations in the system.

To overcome these limitations, a novel bridge damage detection method integrating Discrete Wavelet Transform with Principal Component Analysis (PCA) is introduced. PCA is leveraged to strip environmental effects from vibration responses[17] and eliminate features that are sensitive to damage[18-21]. Yan et al.[22,23] demonstrated PCA’s capability to distinguish damage from environmental variations under both linear and weakly nonlinear conditions. Sen et al.[24] used PCA to detect temporal damage of the structures under the action of environmental change. Huang et al.[25] adopted PCA to extract the data for sensor-fault detection. This approach identifies and isolates faults associated with sensor bias and drift effectively. For sensor fault detection, Kerschen et al.[26] leveraged PCA to model structural monitoring data, defining the index in subspaces as a diagnostic feature. However, PCA-based methods alone are insufficient for accurately localizing structural damage.

Therefore, this method takes into account the advantages of PCA and DWT in damage detection with limited sensors. Firstly, the component matrix of structural response is obtained by PCA. Nie et al.[27] found that each column of the component matrix consists of one order of structural mode shape and the

[1] College of Mechanics and Construction Engineering, Jinan University, Guangzhou 510632, China. [2] Dongguan University of Technology, Dongguan 523808, China. [3] Huizhou Branch of China Tower Company Limited, Huizhou 516003, China. [4] Guangzhou Polytechnic University, Guangzhou 511483, China.

✉ Corresponding author. E-mail: niezh@jnu.edu.cn

Received: August 17, 2024; Revised: November 26, 2024; Accepted: June 25, 2025

corresponding structural dynamic components at this modal frequency. On the basis of this physical interpretation, DWT is used to extract the approximate coefficients of the first dynamic component to reconstruct signals. Finally, the damage can be identified by analyzing the reconstructed signals before and after damage. This paper is organized in five sections. It begins with the detection methodology in Section 2. This is followed by a numerical simulation in Section 3, and subsequently, an experimental validation on a steel bridge in Section 4. The study concludes with the findings in Section 5.

2 Methodology

2.1 Dynamic analysis of a beam bridge under a moving load

Figure 1 demonstrates the analytical model of a beam bridge during loading. The system can be mathematically represented as[28-30]:

$$EI\frac{\partial^4 u}{\partial x^4}+\rho\frac{\partial^2 u}{\partial t^2}+c\frac{\partial u}{\partial t}=f\cdot\delta(x-vt) \tag{1}$$

where x and t represent the distance and the time of the moving load from the left of the bridge. $E, I, u, \rho, c,$ are the Young's modulus, moment of inertia, vertical displacement, the mass in unit length, damping of the bridge, respectively. f and v are the external load and the velocity of the load. $\delta(x)$ represents the Dirac function.

Through modal superposition principles, the vertical displacement u is expressed mathematically as

$$u(x,t)=\sum\nolimits_{n=1}^{\infty}q_n(t)\,\varphi_n(x) \tag{2}$$

where $\varphi_n(x)$ is the nth mode shape and $q_n(t)$ is modal coordinate of the nth mode shape.

Substituting Eq. (2) into Eq. (1), considering the modal orthogonality and $\varphi_n(x)=\sin\dfrac{n\pi x}{L}$, Eq. (1) can be simplified as

$$q_n''(t)+2\xi_n\omega_n q_n'(t)+\omega_n^2 q_n(t)=\frac{2f}{\rho L}\sin\Omega_n t \tag{3}$$

where ξ_n is the damping ratio at the nth modal frequency, ω_n is the nth natural frequency, L is the length of the structure and Ω_n is the nth frequency of the moving load.

By applying the initial conditions $(q_n(t=0)=\dot{q}_n(t=0)=0)$, the general solution is obtained. This yields the vertical displacement response which is given by[27]

$$\begin{aligned}u(x,t)=&\frac{2f}{\rho L}\sum\nolimits_{n=1}^{\infty}\frac{1}{\omega_n^2[(1-S_n^2)+(2\xi_n S_n)^2]}\{(1-S_n^2)\sin\Omega_n t\\&-2\xi_n S_n\cos\Omega_n t+e^{-\xi_n\omega_n t}[2\xi_n S_n\cos\omega_{d_n}t+\frac{S_n}{\sqrt{1-\xi_n^{\ 2}}}(2\xi_n^{\ 2}\\&+S_n^{\ 2}-1)\sin\omega_{d_n}t]\}\sin\frac{n\pi x}{L}\end{aligned} \tag{4}$$

where $S_n=\dfrac{\pi v}{L\omega_n}$ and ω_{d_n} is the nth damping vibration frequency, $\omega_{d_n}=\omega_n\sqrt{1-(\dfrac{c}{2\rho\omega_n})^2}$.

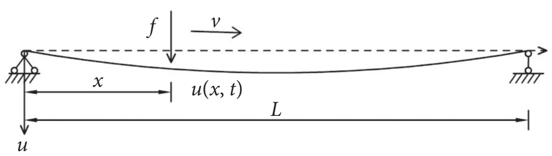

Fig. 1 The simplified bridge model.

2.2 Principal component analysis

PCA facilitates dimensionality reduction from high-dimensional datasets to lower-dimensional representations, preserving essential information characteristics during this conversion process. The data $Z_{a\times b}$ represents the data of the length of a sampling points measured by b sensors, which is performed by

$$Z_{a\times b}=\begin{bmatrix}x_{11}&\cdots&x_{1b}\\\vdots&\ddots&\vdots\\x_{a1}&\cdots&x_{ab}\end{bmatrix} \tag{5}$$

The covariance matrix $\boldsymbol{C}$ of the matrix $\boldsymbol{Z}$ can be expressed as

$$\boldsymbol{C}=\frac{1}{a}(\boldsymbol{Z}-\overline{\boldsymbol{Z}})^{\mathrm{T}}(\boldsymbol{Z}-\overline{\boldsymbol{Z}}) \tag{6}$$

where $\overline{\boldsymbol{Z}}$ is the mean value of each column in $\boldsymbol{Z}$.

The eigenvectors and eigenvalues are derived through the solution of the eigen problem for covariance matrix $\boldsymbol{C}$:

$$\boldsymbol{CV}=\boldsymbol{\Lambda V} \tag{7}$$

where the columns of matrix $\boldsymbol{V}$ are the eigenvectors of the covariance matrix, and $\boldsymbol{\Lambda}$ is a diagonal matrix containing the corresponding eigenvalues, λ_n, which are arranged in descending order.

The component matrix of the original data $\boldsymbol{Z}$ has the following relationship:

$$\boldsymbol{G}^{(n)}=\boldsymbol{Z}\boldsymbol{V}^{(n)} \tag{8}$$

where the nth column of the component represents the nth component.

Principal component analysis is employed to process responses under negligible damping conditions. The derived component matrix formulation is expressed as[27]:

$$\boldsymbol{G}=\frac{2f}{\rho L}\begin{pmatrix}\dfrac{1}{\omega_1^2}\cdot\left(\mathbf{sin}\dfrac{\pi vt}{L}-\dfrac{\pi v}{L\omega_1}\mathbf{sin}\omega_1 t\right)\\\vdots\\\dfrac{1}{\omega_b^2}\cdot\left(\mathbf{sin}\dfrac{b\pi vt}{L}-\dfrac{\pi v}{L\omega_b}\mathbf{sin}\omega_b t\right)\end{pmatrix}^{\mathrm{T}},t=t_1,\cdots,t_a \tag{9}$$

An important interpretation can be found from Eq. (9): the nth column of matrix $\boldsymbol{G}$ comprises both the modal component and dynamic components of the structure. Specifically, the modal component is characterized by $\dfrac{n\pi vt}{L}$, while the dynamic parameters correspond to the vibrational behavior at angular frequency ω_n.These elements collectively represent the mode shape characteristics and time-domain dynamic response of the structure at its modal frequency. To extract each dynamic component from matrix $\boldsymbol{G}$, this paper employs the Moving Average Filter (MAF)[31], which filters the signal at the specific frequency.

$$\mathrm{MAF}(G)=\overline{G(t,n)}=\frac{f_n}{f_s}\sum\nolimits_{j=t-K/2}^{j=t+K/2}G(t,n),n=1,\cdots,b \tag{10}$$

where f_n is the bridge at the nth modal frequency, f_s is the sampling frequency, and K is the length of the MAF calculated by f_s/f_n. According to the physical interpretation of $\boldsymbol{G}$, the nth mode shape can be obtained as:

$$\varphi_n(t)=\mathrm{MAF}\left(G^{(n)}(t)\right) \tag{11}$$

where φ_n is the modal at the nth modal frequency.

The nth dynamic component of the structure is derived by subtracting its corresponding mode from the associated principal component in $G^{(n)}(t)$:

$$d_n(t) = G^{(n)}(t) - \varphi_n(t) \tag{12}$$

It has been demonstrated the first dynamic component primarily contributes to the response of the bridge[27]. Consequently, the first dynamic component is utilized for damage detection using DWT in the subsequent sections.

2.3 Discrete wavelet transform

The wavelet transform along with the theory enabling signal analysis at varying resolutions across different frequency scales, was introduced by Morlet and Grossman in 1980[32-34]. Its mathematical representation is given by the following equation:

$$\mathrm{WT}(\theta,\tau) = \frac{1}{\sqrt{\theta}}\int_{-\infty}^{\infty} Z(t) * \psi\left(\frac{t-\tau}{\theta}\right)\mathrm{d}t \tag{13}$$

where θ is the scaling factor, τ is the shifting factor, and ψ is the mother wavelet.

To enhance the efficiency and accuracy of the algorithm, DWT is expressed as

$$\mathrm{DWT}(h,\sigma) = \frac{1}{\sqrt{2^h}}\int_{-\infty}^{\infty} Z(t) * \psi\left(\frac{t-2^h\sigma}{2^h}\right)\mathrm{d}t \tag{14}$$

where h is the scaling factor and σ is the shifting factor. By substituting the parameter $d_n(t)$ into the Eq. (14), the wavelet coefficient can be obtained.

DWT employs filters to decompose signals into multi-level wavelet coefficients. The output of the low-pass and high-pass filters are termed the approximate and detail coefficients, respectively[35,36]. The approximate coefficient captures the low-frequency information, which reflect characteristics of the structure. By extracting the approximate coefficient to reconstruct the signal, it is vital to retain the important damage information of the structure to localize the damage. In structural damage detection, the dynamic response contains a lot of multi-frequency information and noise, so the signal characteristics are very irregular. To select a suitable wavelet function, it is necessary to take into consideration the characteristics of the response and the impact of the environment comprehensively. By comparing the characteristics of various wavelet functions and the effectiveness of the detection, this method selects the daubechies wavelet function and performs 5-layer wavelet decomposition to extract wavelet coefficients. Finally, five approximate coefficients are selected to reconstruct the signal by comparing the reconstruction effectiveness of the number of wavelet coefficients.

2.4 Damage detection using PCA and DWT based on limited sensors

The displacement under a moving load is measured using a limited sensor array, which is performed by PCA and DWT. The damage information is reflected in the displacement response when the damage occurs. However, it is difficult to detect damage only by changes in response. The response change caused by damage will be captured by dynamic components. In order to improve the sensitivity of the detection, DWT is applied to the dynamic component including angular frequency to extract wavelet coefficients, which compose of the important damage information of the structure. Wavelet coefficients are reconstructed to extract damage index that is sensitive to damage. The reconstruction signal is compared with the reconstruction signal in the healthy state when the damage occurs so the situation of the structure will be judged. Therefore, PCA is applied to get the first dynamic component. Then the DWT is performed on the first dynamic component to obtain the approximate coefficient to reconstruct the signal. Finally, the damage index is defined by analyzing the reconstructed signals to identify the damage location.

The approximate coefficient extracted by DWT using the first dynamic component of the structure is reconstructed as

$$S = \sum\nolimits_{a\in m} A(m)L(a-2m) \tag{15}$$

where S is the reconstructed signal, A is the approximate coefficient, m is the scaling factor, and L is the low-pass filter.

Then the damage index of dynamic component (DIDC) is defined as

$$\mathrm{DIDC} = S^{\mathrm{h}} - S^{\mathrm{d}} \tag{16}$$

where S^{h} and S^{d} are the reconstructed signals of the dynamic component in the healthy state and damaged state, respectively.

A comparison of the reconstructed signals before and after damage enables the localization of damage. This method can realize the matrix calculation of PCA using two sensors. A brief description of the procedure is provided in Figure 2, with the steps detailed as follows:

1) Displacement signals $\boldsymbol{Z}$ are collected for both the healthy and damaged states.

2) PCA is performed on the displacement signals $\boldsymbol{Z}$ to obtain the principal component matrix $\boldsymbol{G}$, eigenvector matrix $\boldsymbol{V}$, and eigenvalue matrix $\boldsymbol{\Lambda}$.

3) The first principal component $G^1(t)$ is filtered by MAF to obtain the first dynamic component $d_1(t)$ and the first mode shape $\varphi_1(t)$. The first principal component is processed by MAF to extract the first modal, which is subsequently utilized to get the first dynamic component.

4) The first dynamic component $d_1(t)$ is processed by DWT, and approximation coefficient A is obtained.

5) The approximation coefficient A is reconstructed to obtain the reconstruction signal S.

6) By calculating the reconstructed signals S in the healthy and damaged state, DIDC is defined to localize the damage.

3 Numerical simulation

To assess the performance of DIDC, a simply supported bridge model is established in ANSYS software. Seven displacement sensors labeled as S1 to S7 are evenly placed, capturing displacement responses during loading. The simplified bridge is illustrated in Figure 3. The structural parameters are defined as follows: L = 20 m, h = 0.2 m, b = 0.1 m, E = 200 GPa and ρ = 7,850 kg/m^3. A moving mass of 1,000 kg traverses the beam at diffferent velocities (v_1=0.5 m/s and v_2=1 m/s). The displacement is sampled at 200 Hz. Structural damage was introduced through the deletion of finite elements at the bottom section. The damage severity is quantified as the ratio of deleted elements to the total elements within the cross-section. The model is divided into ten sub-units along the height direction of the bridge. It represents the damage severity of 10% while deleting a unit. The damage location is counted from the left.

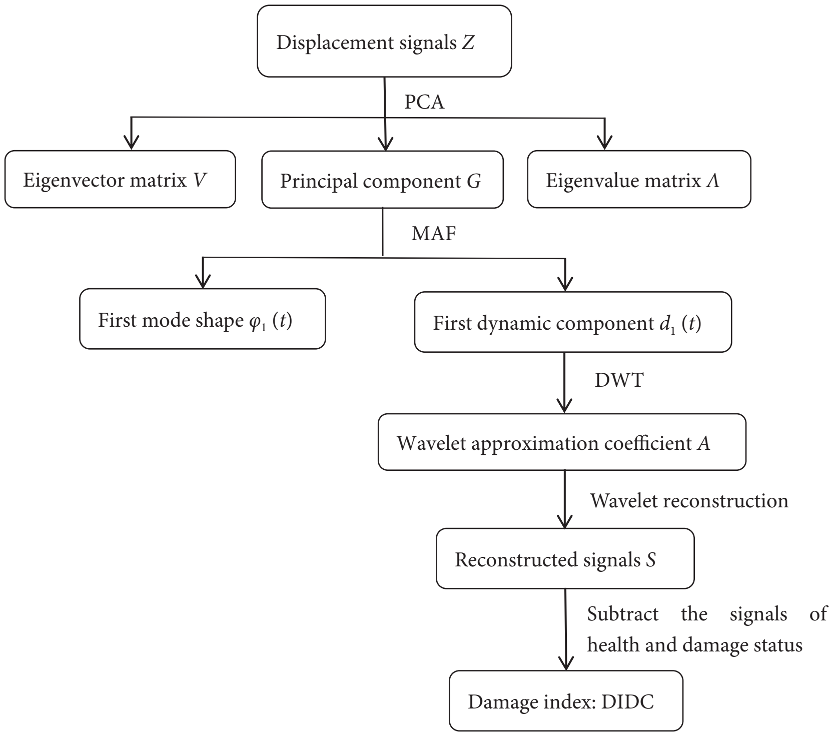

Fig. 2 Flowchart of the proposed method.

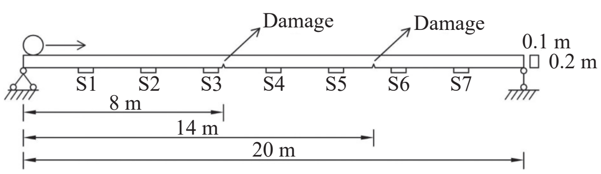

Fig. 3 The simply supported beam bridge model.

3.1 Single damage

3.1.1 Scenarios of different damage severities

The single damage simulation scenario is presented in Table 1. The damage severity defined as the percentage loss of the cross-section area in the structure is set at 10%, 20%, and 30%, with the damage location of L_d= 0.4L. A triangle on the horizontal axis corresponds to the damage. The scenario set as L_d=0.4L with the damage severity of 10% at the speed of v_1 is taken as an example.

Figure 4 presents the first dynamic component with its corresponding Fourier spectrum, revealing the natural frequency of 1.12 Hz. It is difficult to detect damage only by the change of the dynamic component. The displacement response gathered from the seven sensors serves as the input for the DIDC computation. Figure 5 shows a peak in the DIDC curve at 0.4L under different speeds, validating the given damage location. And MAF is a moving windowing method, which will blur the average value at the boundary leading to the boundary effect of DIDC. The same phenomenon appears in later results so it will not be described again. The results verify that DIDC is robust to detect the location at varying damage severities and speeds. Furthermore,

Table 1 The scenario setting of single damage.

Damage location	Damage severity (%)
L_d = 0.4L	10, 20, 30
L_d = 0.7L	10, 20, 30

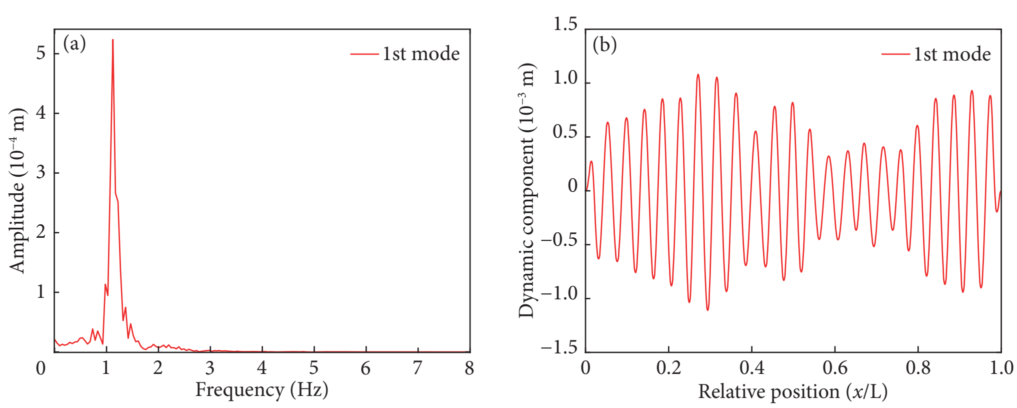

Fig. 4 First dynamic component and the corresponding Fourier spectrum: (a) the first dynamic component, (b) Fourier spectrum.

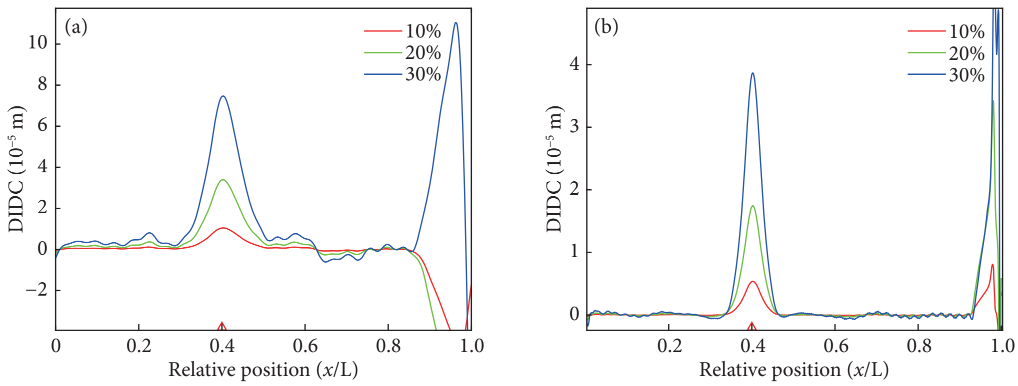

Fig. 5 Results with different severities at L_d= 0.4*L*: (a) moving mass at v_1, (b) moving mass at v_2.

it is observed that the peak value associated with the damage location rises as the severity increases. However, the method proposed will fail when the damage occurs near the boundaries of the bridge.

Furthermore, an assessment of the method's effectiveness across various damage locations was also performed. Damage severities of 10%, 20%, and 30% are set at L_d=0.7L, with the results presented in Figure 6. It is evident for all severities that corresponding curves have clear peaks at L_d=0.7L, which corresponds to the introduced damage. Increasing the speed to v_2, the method remains effective to accurately detect the damage. These findings demonstrate DIDC is capable of reliably detecting the damage.

In traditional methods, researchers often extract wavelet coefficient as an index to detect the damage using the response directly. Figure 7 shows the method using wavelet coefficient can not detect the damage location. This is because that dynamic response is the linear superposition of multimodal dynamic information. The influence of the wavelet coefficient caused by the fluctuation of the high frequency dynamic components is larger than it caused by the damage. Besides, it is also easily affected by the noise[14]. However, in the proposed method of this paper, the high-frequency dynamic components and noise are filtered out but remaining the first dynamic component using the PCA, leading to avoiding the interference from high-frequency components and noise. The comparative analysis reveals that the method achieves effective damage localization, whereas the wavelet coefficient alone proves insufficient. The performance of

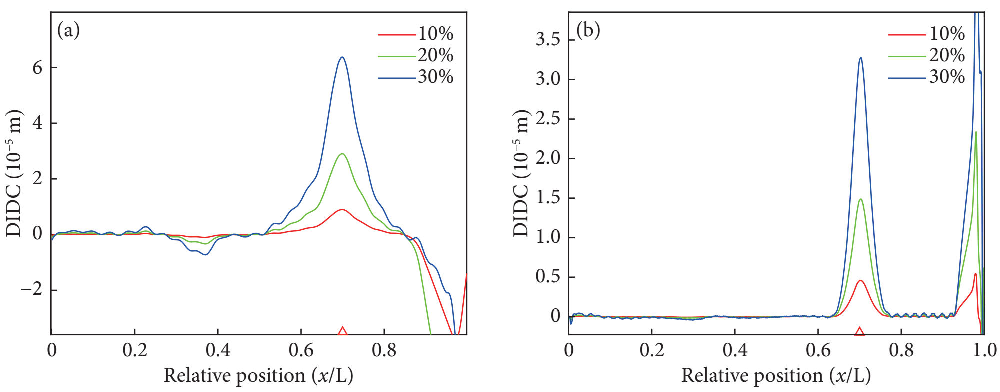

Fig. 6 Results with different severities at L_d= 0.7*L*: (a) moving mass at v_1, (b) moving mass at v_2.

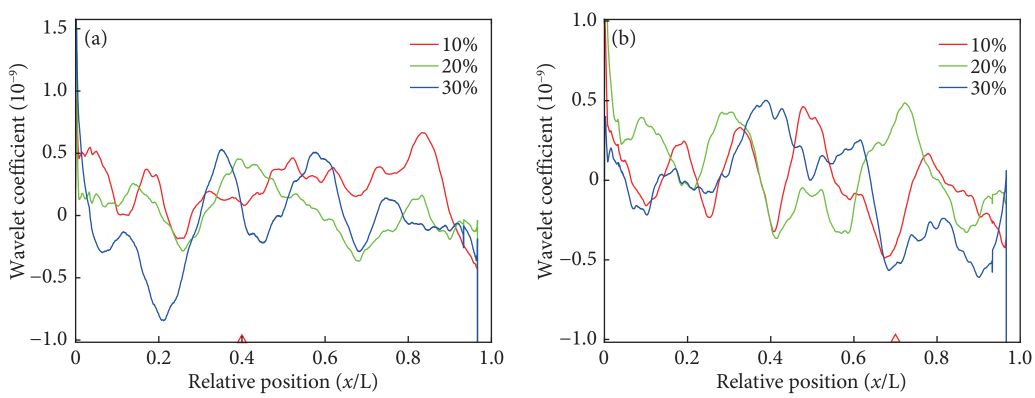

Fig. 7 Detection results using wavelet coefficient at the speed of v_2: (a) 0.4*L*, (b) 0.7*L*.

DIDC depends on the severity of the damage as the peak value at the damage location increases with the severity increases.

3.1.2 Results using limited sensors

To assess the method in damage detection with fewer sensors, three scenarios are examined as detailed in Table 2. For Case 1, damage detection is carried out using five sensors (S1, S3, S4, S5, S7), with all parameters remaining the same as the previous section. The results of different locations are shown in Figure 8 and Figure 9. Then, the number of sensors is reduced again and only two sensors (S2, S6 and S3, S5) are selected. The results are shown in Figures 10–13. All DIDC curves have a peak at $0.4L$ or $0.7L$, indicating that this method has good performance when using limited sensors even only two sensors are used in Case 2 and Case 3. Despite a reduction in the number of sensors, DIDC can also detect the damage because the first dynamic component can be extracted well by PCA with several sensors, whether it is 2 or 4 sensors. However, comparing the results in Case 1 to 3, as the number of sensors decreases, the peak value of DIDC decreases, resulting from the decrease of damage information because less information is used. The least number of sensor used in this

Table 2 The scenario setting of sensor combinations.

Case	Sensor combination
1	S1, S3, S4, S5, S7
2	S2, S6
3	S3, S5

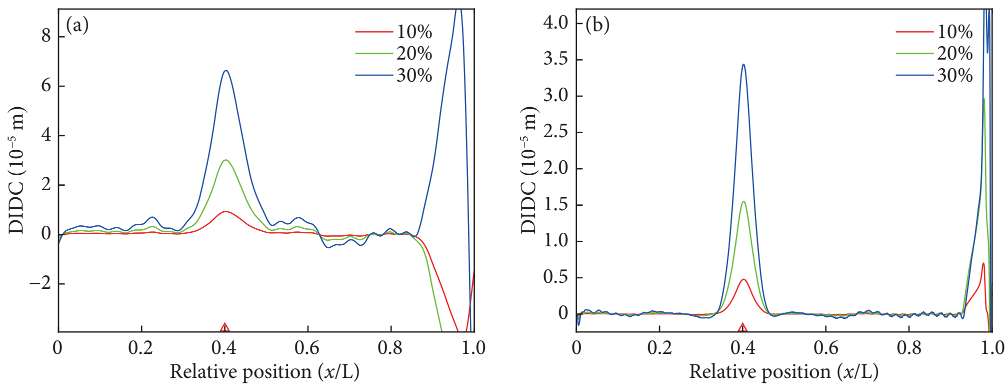

Fig. 8 Damage detection results in Case 1 at L_d= 0.4L: (a) moving mass at v_1, (b) moving mass at v_2.

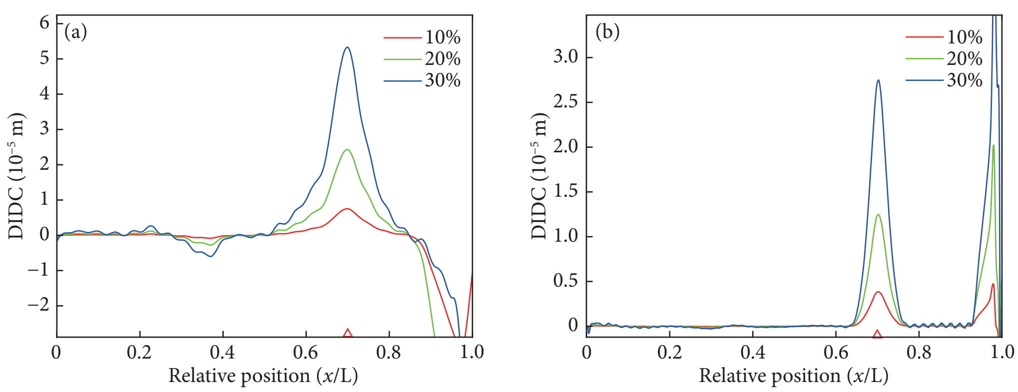

Fig. 9 Damage detection results in Case 1 at L_d= 0.7L: (a) moving mass at v_1, (b) moving mass at v_2.

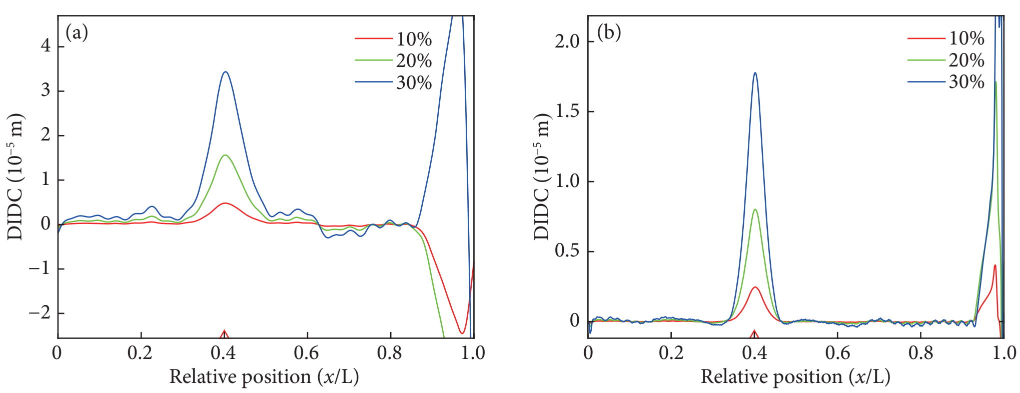

Fig. 10 Results in Case 2 at L_d= 0.4L: (a) moving mass at v_1, (b) moving mass at v_2.

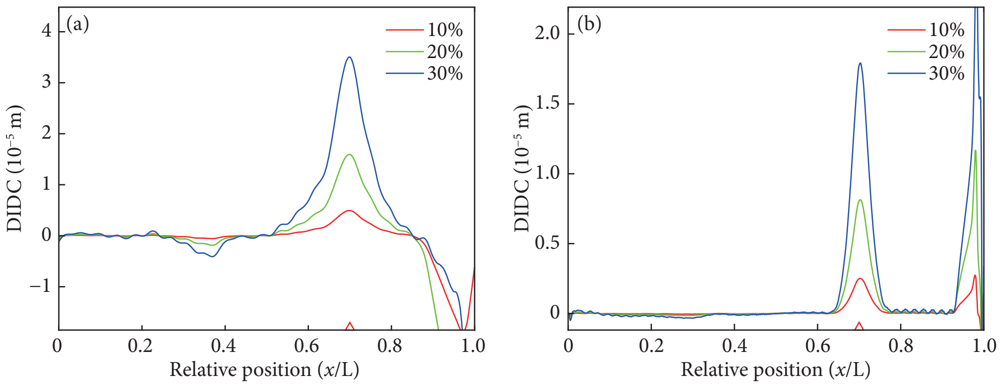

Fig. 11 **Damage detection results in Case 2 at L_d= 0.7L: (a) moving mass at v_1, (b) moving mass at v_2.**

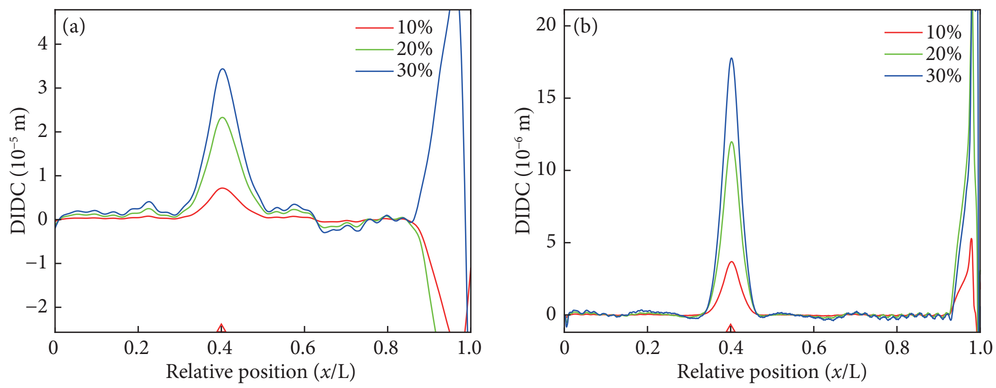

Fig. 12 **Damage detection results in Case 3 at L_d= 0.4L: (a) moving mass at v_1, (b) moving mass at v_2.**

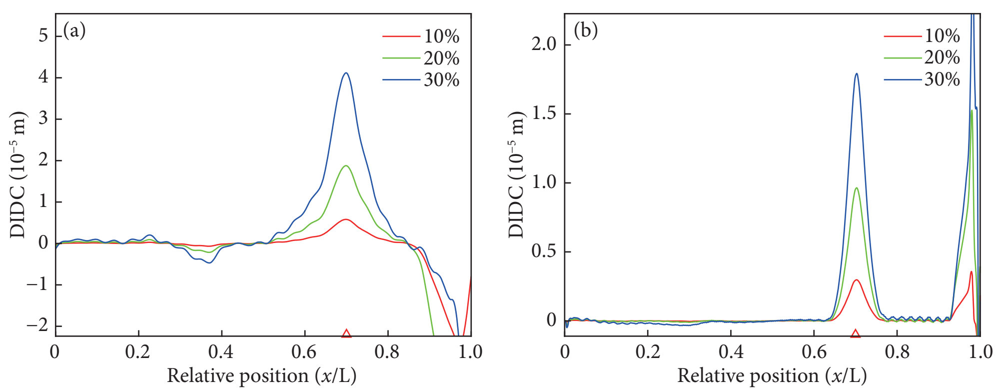

Fig. 13 **Damage detection results in Case 3 at L_d= 0.7L: (a) moving mass at v_1, (b) moving mass at v_2.**

method is two, because the process of the first dynamic component extraction is a matrix operation. We need at least two sensors to measure the structural responses to form a data matrix.

3.2 Multiple damage

Scenarios of multiple damage detection are performed. MD including two damage locations L_d = 0.4L and L_d = 0.7L are considered here. Scenarios of multiple damage including MD1 and MD2 are defined, as shown in Table 3. Firstly, DIDC is calculated by using the displacement response obtained by seven sensors. Figure 14 reveals distinct peaks at each imposed damage position, indicating precise and effective localization of DIDC. To verify the effectiveness of the scenario including the degrees of damage at different locations varying, 0.4L is set as damage severity of 20% and 0.7L is set as damage severity of 40% that is defined as MD3. Figure 15 shows DIDC still maintains robustness to detect different degrees at different locations. When the vehicle is set at v_2, DIDC remains effective in detecting damage. The results indicate that DIDC can detect damage across varying

Table 3 **The scenario setting of multiple damage.**

Damage location	Damage severity	
	MD1 (%)	MD2 (%)
L_d = 0.4L	20	40
L_d = 0.7L	20	40

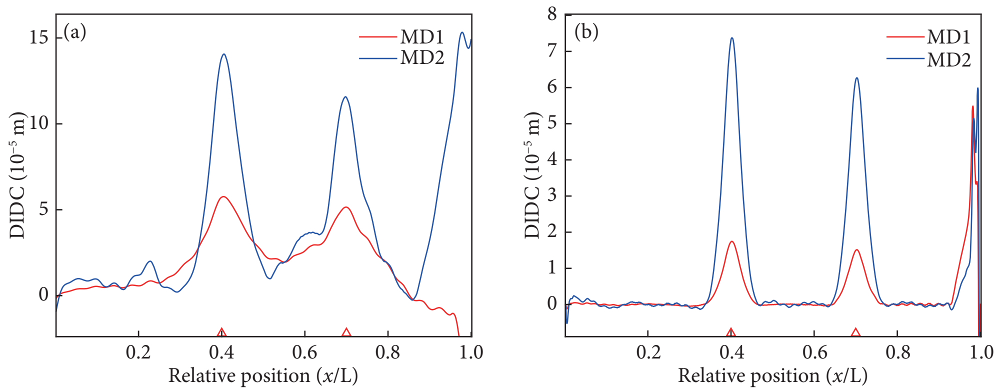

Fig. 14 **Results of multiple damages with different severities: (a) moving mass at v_1, (b) moving mass at v_2.**

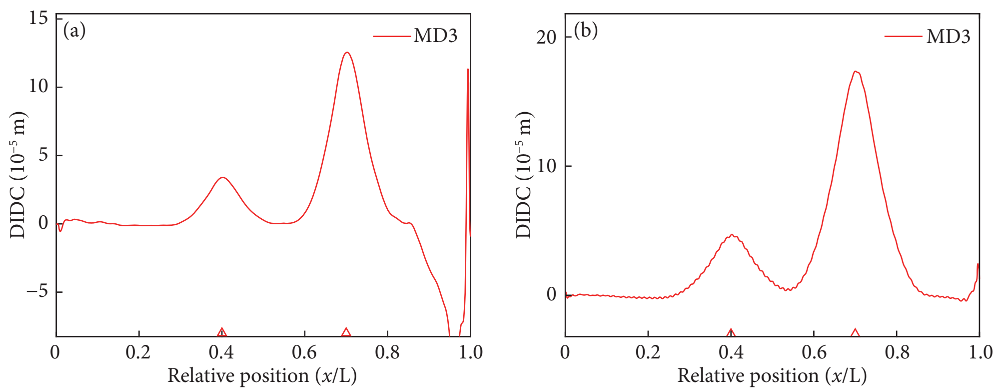

Fig. 15 **Detection results at different locations with different damage severities: (a) moving mass at v_1, (b) moving mass at v_2.**

severities in MD1 and MD2, with the peak at the location rising as the severity increases.

To evaluate the effectiveness of DIDC using limited sensors in this session, the sensor combinations in Table 2 are investigated again. Figures 16–18 show DIDC have obvious peaks at 0.4*L* and 0.7*L*, no matter using five sensors in Case 1 or two sensors in Cases 2 and 3. These results indicate that DIDC also maintains robustness in multiple damage detection by using limited sensors. These results are similar to that of using all the seven installed sensors shown in Figure 14 but the sensitivity of the index also decreases when reduce the used sensor number. But the decrease of sensitivity do not affect the judgment in detection. DIDC is calculated based on the dynamic component including oscillation information, so oscillations of DIDC will also occur in the non-damage position. However, the oscillation caused by non-damage position is smaller than the oscillation information created by damage, which does not affect the effectiveness of damage detection.

3.3 Robustness to noise

To evaluate the method's robustness to noise, Gaussian noise of different levels is applied to the displacement response. The signal-to-noise ratio (SNR) is employed to evaluate the noise, as defined below[37]:

$$\mathrm{SNR} = 10\lg\frac{P_x}{P_{\mathrm{N}}} \tag{17}$$

where P_x is the power of the displacement, and P_{N} is the power of the measurement noise.

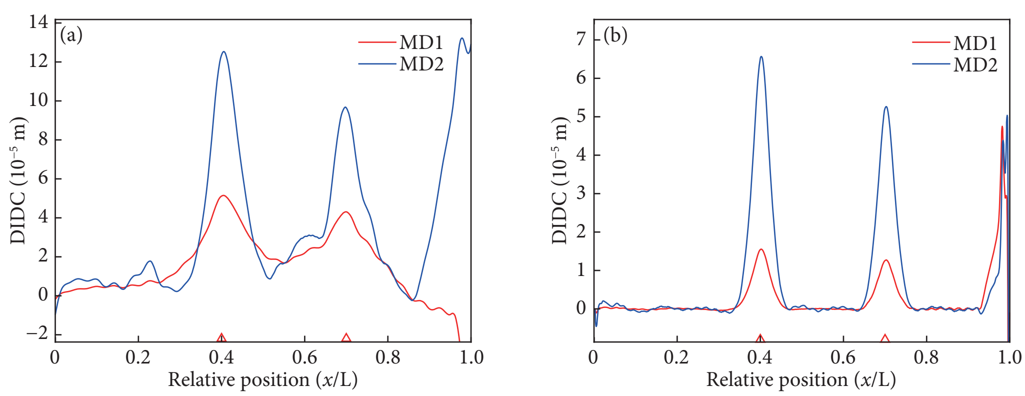

Fig. 16 **Results of multiple damage detection in Case 1: (a) moving mass at v_1, (b) moving mass at v_2.**

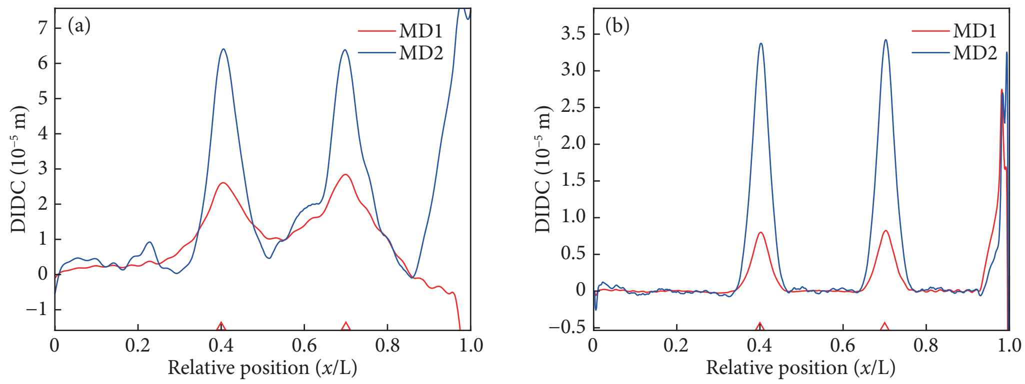

Fig. 17 Results of detection in Case 2: (a) moving mass at v_1, (b) moving mass at v_2.

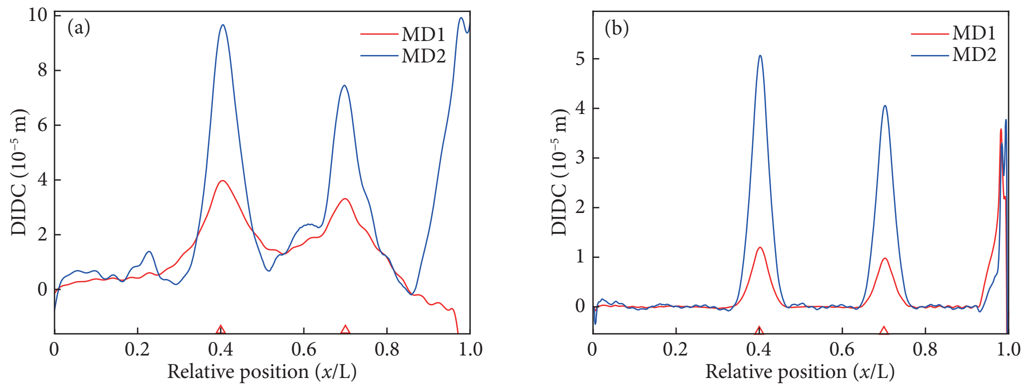

Fig. 18 Results of multiple damage detection in Case 3: (a) moving mass at v_1, (b) moving mass at v_2.

The SNRs are set at 40 dB and 25 dB, respectively. The displacement response of healthy state at v_2 and the signal with 40 dB are presented in Figure 19. The damage is considered at 0.4L, with the vehicle velocity set at different speeds. The results of DIDC at the noise level of 40 dB are presented in Figure 20. As shown, the result remains remarkably stable, showing no significant difference from the case in Figure 7. This robustness is maintained even at a higher noise level of 25 dB, as demonstrated in Figure 21. As shown, the results are also similar to that of non-noise scenario except for the slight variations at the non-damaged location. It can still identify the damage which shows that DIDC has good robustness to noise. This is because that the PCA method itself has a denoising function by projecting the noise onto the high order of principal component vector which is neglected but not affect the extraction of the dominant first principal component.

4 Experimental verification

4.1 Experimental setup

A hollow steel beam bridge is tested to further assess the performance of this method. Five electrical eddy current sensors are placed uniformly along the length of the bridge to measure the displacement response, with sensors represented by S1 to S5 from the left to the right. The simplified model is shown in Figure 22. The beam bridge is a hollow rectangular section with the width of 200 mm, the height of 100 mm and the thickness of 3 mm. The length and the density of the beam are 6 m and 7,850 kg/m^3. A

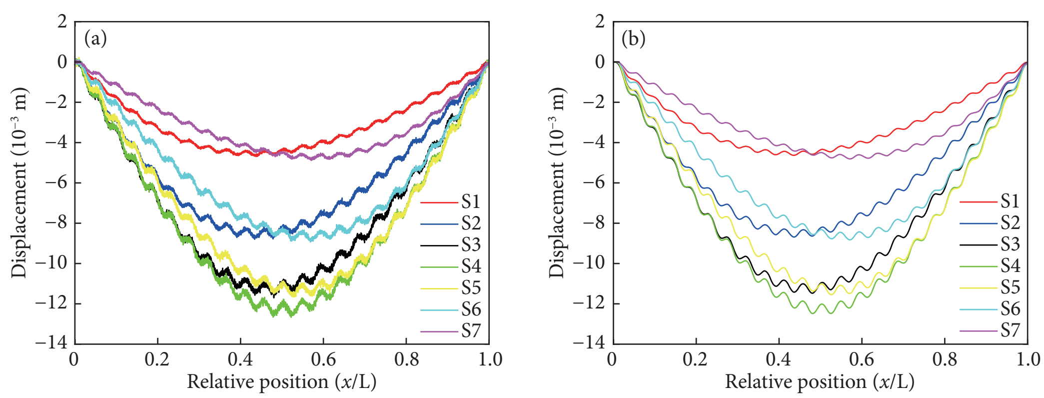

Fig. 19 Displacement responses at the healthy state with 1 m/s and the signal with the noise with 40 dB: (a) Displacement, (b) the signal with 40 dB.

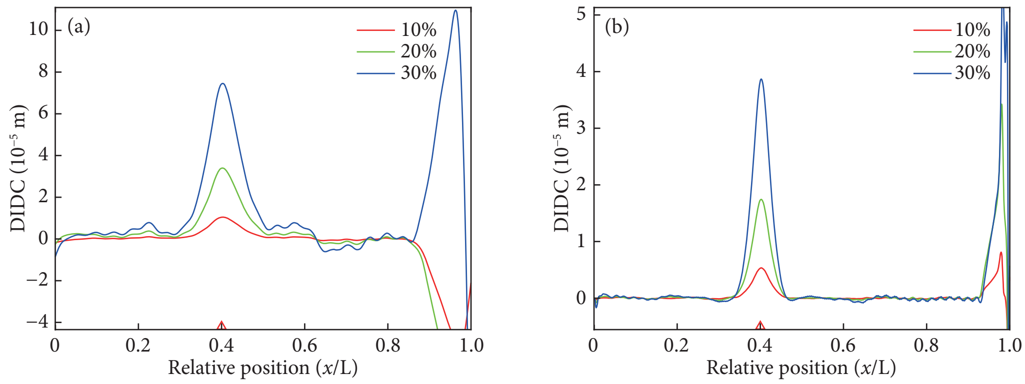

Fig. 20 Results with different severities under 40 dB: (a) moving mass at v_1, (b) moving mass at v_2.

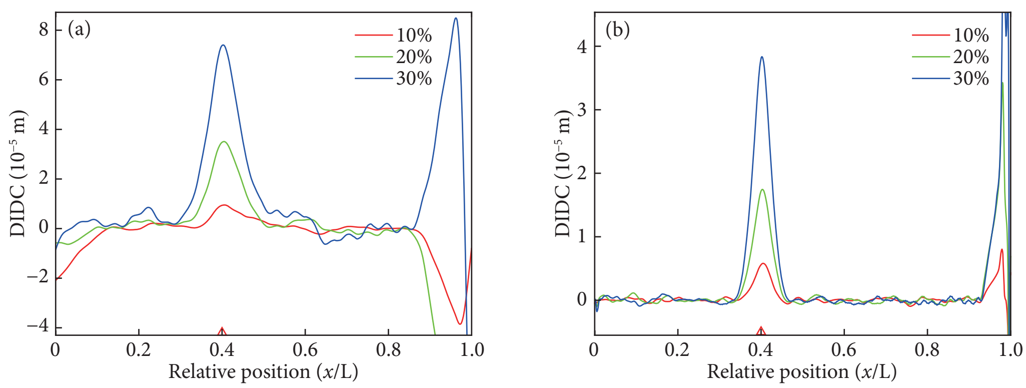

Fig. 21 Results of different severities under 25 dB: (a) moving mass at v_1, (b) moving mass at v_2.

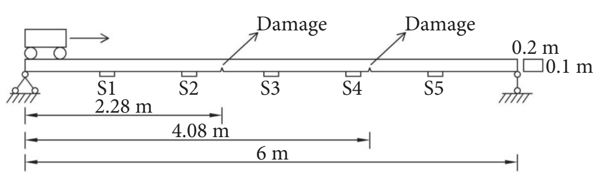

Fig. 22 Experimental schematic diagram.

four-wheeled vehicle with 10.5 kg propelled by a DC motor traversed the bridge at different speeds (v_3 = 0.5 m/s and v_4 = 0.75 m/s) along steel angle rails. Response data is acquired with a DH5922N system at 500 Hz. Damage scenarios in Table 4 are created by cutting notches at the bottom, with the experimental configuration shown in Figure 23.

4.2 Results of single damage

Take SD1 with a speed of v_4 as an example. The signals collected by the five sensors and the corresponding Fourier spectrum are shown in Figure 24, which shows the natural frequency is 9.75 Hz. And the first dynamic component is shown in Figure 25. It is difficult to detect damage only by the change of the displacement and the first dynamic component.

Figure 26 shows the results with the five sensors installed at different speeds. As demonstrated, the damage can be accurately

Table 4 Experimental damage scenarios.

Damage location	Depth of crack				
	SD1	SD2	SD3	MD1	MD2
$L_d = 0.38L$	–	–	–	4 mm	7 mm
$L_d = 0.68L$	3 mm	5 mm	7 mm	7 mm	7 mm

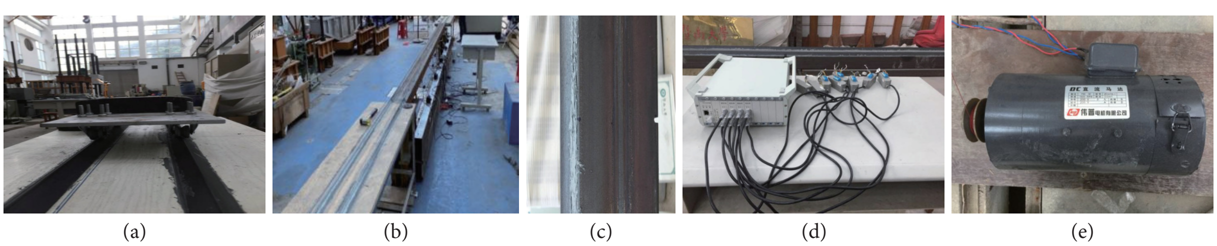

Fig. 23 Experimental setup: (a) beam bridge, (b) model vehicle, (c) crack, (d) DH5922N dynamic system, (e) direct-current motor.

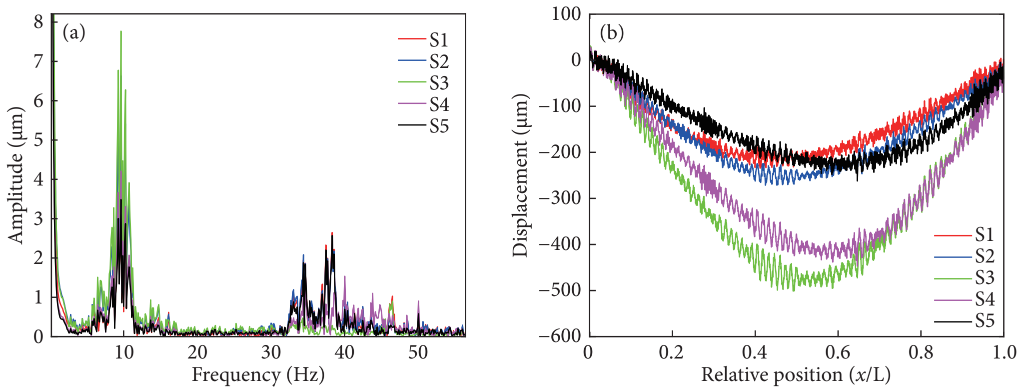

Fig. 24 Response characteristics of scenario SD1 at v_4: (a) time-domain displacement, (b) frequency-domain Fourier spectrum.

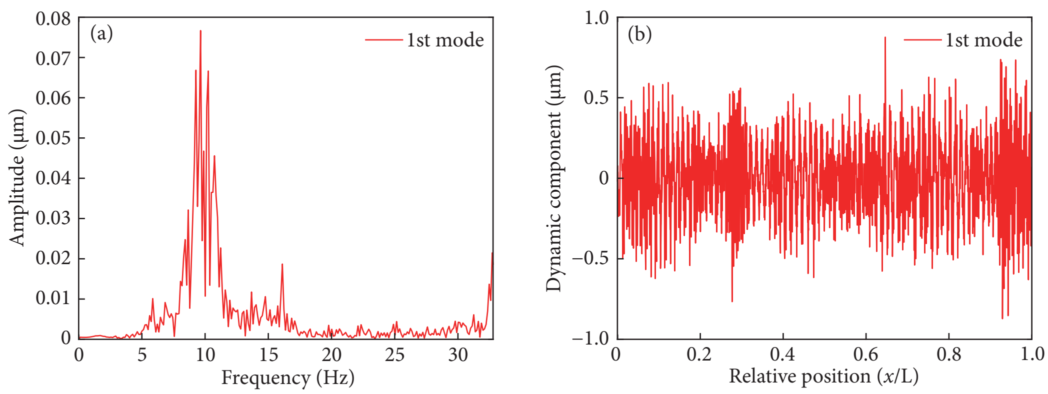

Fig. 25 First dynamic component and the corresponding Fourier spectrum: (a) the first dynamic component, (b) Fourier spectrum.

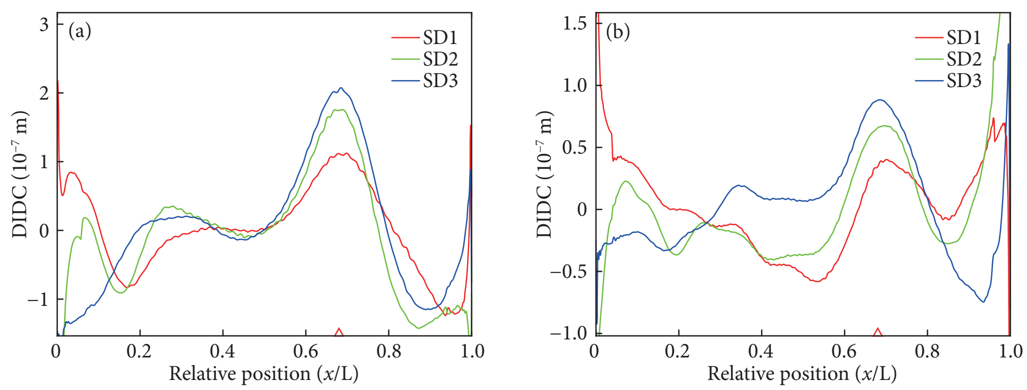

Fig. 26 Results with different severities: (a) vehicle speed at v_3, (b) vehicle speed at v_4.

and confidently localized. And the boundary effect results from MAF and other environmental factors. Compared with simulation results, it can be observed from the experimental results that the damage peak increases with severity, and the DIDC method successfully detects this damage.

To assess the effectiveness of DIDC while reducing the number of sensors, detection is conducted using different sensor combinations including four sensors (S1, S2, S4, S5) and two sensor pairs (S2, S4 and S1, S5), as described in Table 5. The detection results with different vehicle speeds using these sensor combinations, are presented in Figures 27–29. The results demonstrate that damage can still be detected when the number of sensor is reduced for single damage detection. DIDC can detect the damage in Case 2 and Case 3, indicating that this method has good performance for detection when using two sensors. This method can detect the damage location because the first dynamic

Table 5 The scenario setting of sensor combinations.

Case	Sensor combination
1	S1, S2, S4, S5
2	S2, S4
3	S1, S5

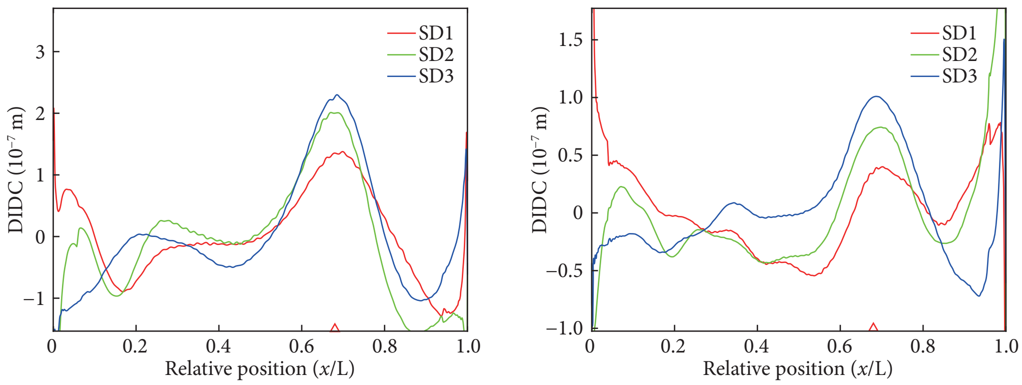

Fig. 27 Results with different severities in Case 1: (a) vehicle speed at v_3, (b) vehicle speed at v_4.

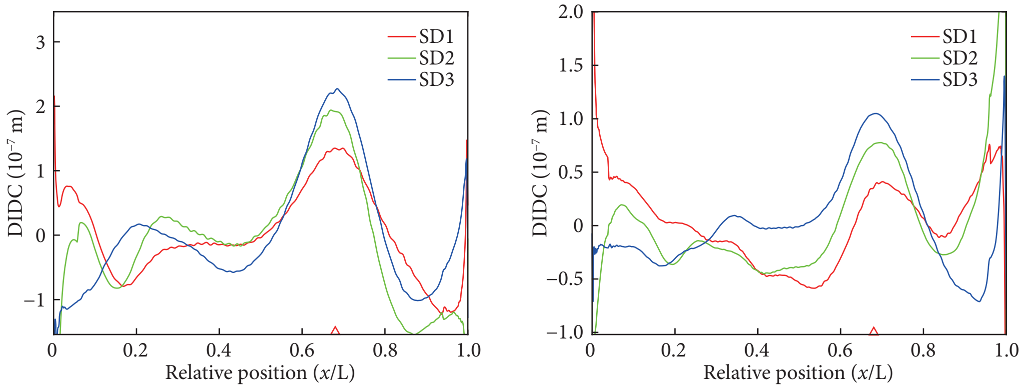

Fig. 28 Results with different severities in Case 2: (a) vehicle speed at v_3, (b) vehicle speed at v_4.

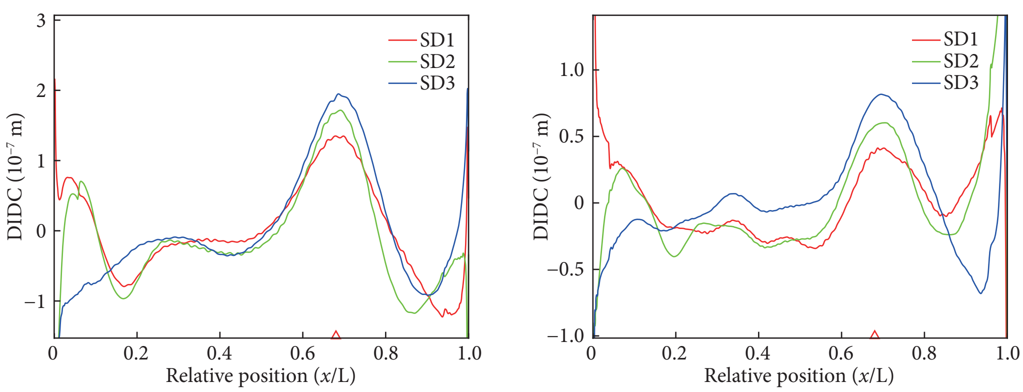

Fig. 29 Results with different severities in Case 3: (a) vehicle speed at v_3, (b) vehicle speed at v_4.

component can be extracted well by PCA with several sensors. The least number of sensor used in this method is two, because the extraction of the first dynamic component involves the matrix operation. At least two sensors are necessary to capture the structural responses and construct a data matrix. Comparing the results of different sensor combinations, the peak of Case 2 is larger than the peak of Case 3 because Case 2 is closer to the damage location. Therefore, the method based on the first dynamic component can detect damage locations of the structure.

4.3 Results of multiple damage

The effectiveness of DIDC in multi-damage detection is further studied. Displacement signals are collected using five sensors and the detection results are presented in Figure 30, which show that DIDC has peaks at the damage locations. For the damage detection process, three sensor combinations are employed: Four sensors (S1, S2, S4, S5) and two sensors (S2, S4 and S1, S5). The results are shown in Figures 31–33. In the scenarios of multiple damage, the peak of the MD2 curve is always larger than MD1 at the damage. The phenomenon is consistent with the expected setting that the damage severities of MD2 is larger than MD1. When the damage occurs in the structure, the dynamic component will change. The change of the damage will be more obvious after performing discrete wavelet transform. So the damage scenario of the structure can be judged by the peak of the DIDC. The curve of DIDC has peaks at other non-damage locations owing to the influence of other factors such as the environment, but there is still the maximum peak at the damaged

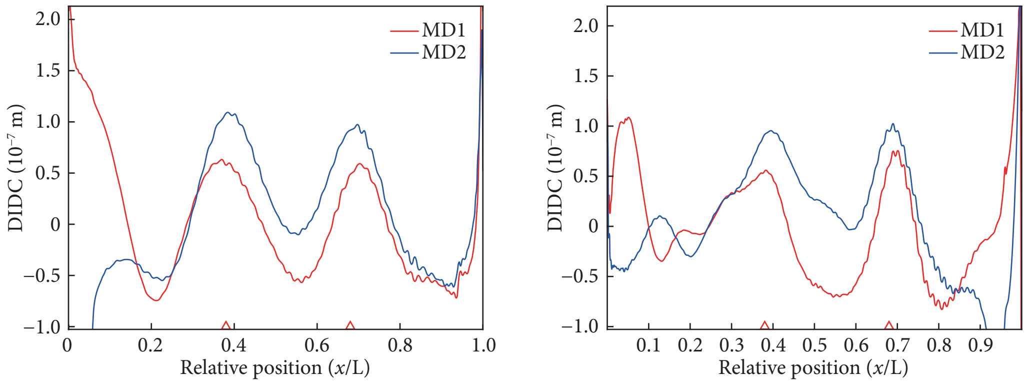

Fig. 30 Results using all sensors: (a) vehicle speed at v_3, (b) vehicle speed at v_4.

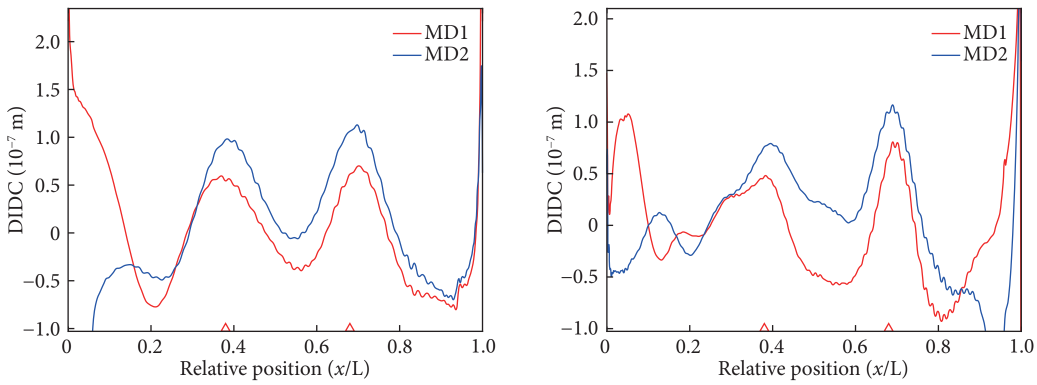

Fig. 31 Detection results of multiple damages in Case 1: (a) vehicle speed at v_3, (b) vehicle speed at v_4.

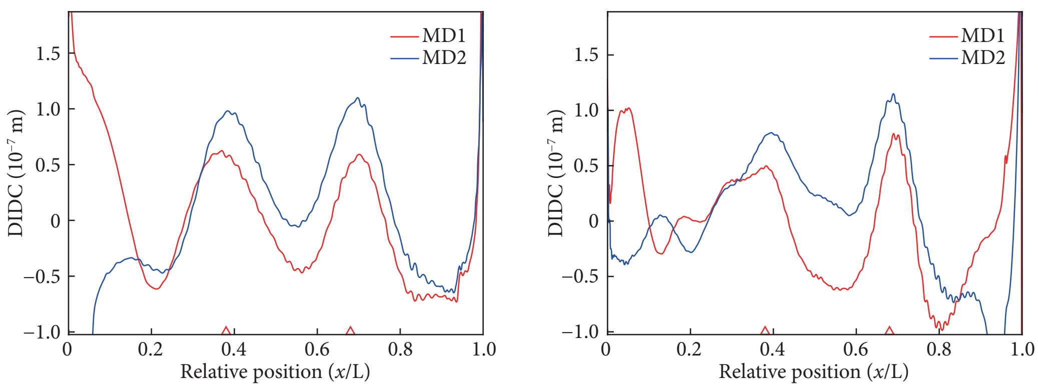

Fig. 32 Detection results of multiple damages in Case 2: (a) vehicle speed at v_3, (b) vehicle speed at v_4.

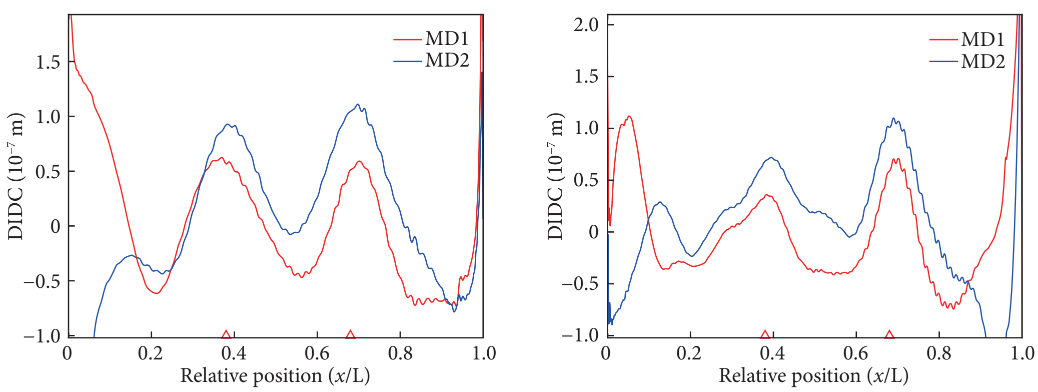

Fig. 33 Detection results of multiple damages in Case 3: (a) vehicle speed at v_3, (b) vehicle speed at v_4.

location. When the vehicle speed increases, the effective information collected by the sensor decreases. However, it does not affect the effectiveness of structural detection. The curve of DIDC show multiple damage can be identified when reducing the number of sensors and increasing the vehicle speed.

5 Conclusions

This paper introduces a novel approach that integrates PCA with DWT for bridge detection. The method effectively localizes structural damage by displacement responses, collected from a limited sensor array under moving load conditions. The displacement data are performed by PCA to extract the principal components, which include both the mode shape and the associated dynamic components of the structure. The dynamic component is extracted by removing the mode shape through a low-pass filter. Then the approximate coefficients of the dynamic component are extracted by DWT to reconstruct the signal, and DIDC is defined on this basis. When the structure is damaged, the damage index DIDC appears a peak at the damage location, so as to detect the damage. To verify the effectiveness of DIDC, a numerical simulation of a beam bridge model and experimental testing on a steel beam bridge are conducted. Both simulation and experiment results show that DIDC can detect damage in different scenarios with limited sensors. This method can reduce the cost of the system and improve the accuracy of the bridge damage detection. It has good robustness to noise and can be applied to practical engineering. In addition, this method is simple in operation and fast in calculation speed, which can improve the efficiency of the detection.

Acknowledgements

This work was financial support by the projects in the National Natural Science Foundation of China under grant number (No. 52178289).

Author contribution statement

Xiaojie Zheng is responsible for Investigation, Software, Writing - original draft. Honghong Li is responsible for Writing - review & editing, Supervision. Zhenhua Nie is responsible for Conceptualization, Writing - review & editing, Supervision. Hongwei Ma is responsible for Conceptualization, Writing - review & editing, Supervision.

Data availability

The data that support the findings of this study is available from the corresponding author upon reasonable request.”

Use of AI statement

None.

Declaration of competing interest

Xiaojie Zheng is the employee of Huizhou Branch of China Tower Company Limited. All the other author(s) have no competing interests to declare that are relevant to the content of this article.

References

[1] Shih, H. W., Thambiratnam, D. P., Chan, T. H. T. (2011). Damage detection in truss bridges using vibration based multi-criteria approach. *Structural Engineering and Mechanics*, 39: 187–206.
[2] Nair, K. K., Kiremidjian, A. S., Law, K. H. (2006). Time series-based damage detection and localization algorithm with application to the ASCE benchmark structure. *Journal of Sound and Vibration*, 291: 349–368.
[3] Zhang, Q. W. (2007). Statistical damage identification for bridges using ambient vibration data. *Computers & Structures*, 85: 476–485.
[4] Adams, R. D., Cawley, P., Pye, C. J., Stone, B. J. (1978). A vibration technique for non-destructively assessing the integrity of structures. *Journal of Mechanical and Engineering Science*, 20: 93–100.
[5] Pandey, A. K., Biswas, M. (1994). Damage detection in structures using changes in flexibility. *Journal of Sound and Vibration*, 169: 3–17.
[6] Durak, L., Arikan, O. (2003). Short-time Fourier transform: Two fundamental properties and an optimal implementation. *IEEE Transactions on Signal Processing*, 51: 1231–1242.
[7] Allemang, R. J. (2003). The modal assurance criterion—Twenty years of use and abuse. *Sound and Vibration*, 37(8): 14–23.
[8] Reda Taha, M. M., Noureldin, A., Lucero, J. L., Baca, T. J. (2006). Wavelet transform for structural health monitoring: A compendium of uses and features. *Structural Health Monitoring*, 5: 267–295.
[9] Bofill, P., Zibulevsky, M. (2001). Underdetermined blind source separation using sparse representations. *Signal Processing*, 81: 2353–2362.
[10] Douka, E., Loutridis, S., Trochidis, A. (2003). Crack identification in beams using wavelet analysis. *International Journal of Solids and Structures*, 40: 3557–3569.
[11] Knitter-Pitkowska, A., Guminiak, M. (2020). Application of 1-D and 2-D discrete wavelet transform to crack identification in statically and dynamically loaded plates. *Engineering Transactions*, 68(2): 137–157.
[12] Zhu, X. Q., Law, S. S. (2006). Wavelet-based crack identification of bridge beam from operational deflection time history. *International Journal of Solids and Structures*, 43: 2299–2317.
[13] Khorram, A., Rezaeian, M., Bakhtiari-Nejad, F. (2013). Multiple cracks detection in a beam subjected to a moving load using wavelet analysis combined with factorial design. *European Journal of Mechanics - A/Solids*, 40: 97–113.
[14] Nguyen, K. V., Tran, H. T. (2010). Multi-cracks detection of a beam-like structure based on the on-vehicle vibration signal and wavelet analysis. *Journal of Sound and Vibration*, 329: 4455–4465.
[15] Sha, G., Radzienski, M., Soman, R., Cao, M., Ostachowicz, W., Xu, W. (2020). Multiple damage detection in laminated composite beams by data fusion of Teager energy operator-wavelet transform mode shapes. *Composite Structures*, 235: 111798.
[16] Xin, C., Wang, C., Xu, Z., Wang, J., Yan, S. (2022). Damage detection of structures from motion videos using high-spatial-resolution mode shapes and data fusion. *Engineering Failure Analysis*, 140: 106560.
[17] Marcoulides, G. A. (2004). The elements of statistical learning: Data mining, inference and prediction. *Structural Equation Modeling-A Multidisciplinary Journal*, 11(1): 150–151.
[18] Mujica, L. E., Rodellar, J., Fernández, A., Güemes, A. (2011). Q-statistic and T2-statistic PCA-based measures for damage assessment in structures. *Structural Health Monitoring*, 10: 539–553.
[19] Tomé, E. S., Pimentel, M., Figueiras, J. (2019). Online early damage detection and localisation using multivariate data analysis: Application to a cable-stayed bridge. *Structural Control and Health Monitoring*, 26: e2434.
[20] Cao, S., Ouyang, H., Cheng, L. (2019). Baseline-free multidamage identification in plate-like structures by using multiscale approach

and low-rank modelling. *Structural Control and Health Monitoring*, 26: e2293.

[21] Nie, Z., Li, F., Li, J., Hao, H., Lin, Y., Ma, H. (2024). Baseline-free structural damage detection using PCA- Hilbert transform with limited sensors. *Journal of Sound and Vibration*, 568: 117966.

[22] Yan, A. M., Kerschen, G., De Boe, P., Golinval, J. C. (2005). Structural damage diagnosis under varying environmental conditions: Part I: A linear analysis. *Mechanical Systems and Signal Processing*, 19: 847–864.

[23] Yan, A. M., Kerschen, G., De Boe, P., Golinval, J. C. (2005). Structural damage diagnosis under varying environmental conditions: Part II: Local PCA for non-linear cases. *Mechanical Systems and Signal Processing*, 19: 865–880.

[24] Sen, D., Erazo, K., Zhang, W., Nagarajaiah, S., Sun, L. (2019). On the effectiveness of principal component analysis for decoupling structural damage and environmental effects in bridge structures. *Journal of Sound and Vibration*, 457: 280–298.

[25] Huang, H. B., Yi, T. H., Li, H. N. (2017). Sensor fault diagnosis for structural health monitoring based on statistical hypothesis test and missing variable approach. *Journal of Aerospace Engineering*, 30: B4015003.

[26] Kerschen, G., De Boe, P., Golinval, J. C., Worden, K. (2005). Sensor validation using principal component analysis. *Smart Materials and Structures*, 14: 36–42.

[27] Nie, Z., Shen, Z., Li, J., Hao, H., Lin, Y., Ma, H. (2022). Output-only complete mode shape identification of bridges using a limited number of sensors. *Mechanical Systems and Signal Processing*, 178: 109246.

[28] Timoshenko, S. P. (1922). CV. On the forced vibrations of bridges. *The London, Edinburgh, and Dublin Philosophical Magazine and Journal of Science*, 43: 1018–1019.

[29] Jeffcott, H. H. (1929). VI. On the vibration of beams under the action of moving loads. *The London, Edinburgh, and Dublin Philosophical Magazine and Journal of Science*, 8: 66–97.

[30] Lowan, A. N. (1935). LIV. On transverse oscillations of beams under the action of moving variable loads. *The London, Edinburgh, and Dublin Philosophical Magazine and Journal of Science*, 19: 708–715.

[31] Nie, Z., Ngo, T., Ma, H. (2017). Reconstructed phase space-based damage detection using a single sensor for beam-like structure subjected to a moving mass. *Shock and Vibration*, 2017: 5687837.

[32] Grossmann, A., Morlet, J. (1984). Decomposition of hardy functions into square integrable wavelets of constant shape. *SIAM Journal on Mathematical Analysis*, 15: 723–736.

[33] Zhao, Q., Li, W., Shao, Y., Yao, X., Tian, H., Zhang, J. (2015). Damage detection of wind turbine blade based on wavelet analysis. In Proceedings of the 2015 8th International Congress on Image and Signal Processing (CISP). Shenyang, China. 1406–1410.

[34] Yao, X., Guo, C., Zhong, M., Li, Y., Shan, G., Zhang, Y. (2009). Wind turbine gearbox fault diagnosis using adaptive morlet wavelet spectrum. In Proceedings of the 2009 Second International Conference on Intelligent Computation Technology and Automation. Changsha, China. 580–583.

[35] Kumar, G., Kumar, A. (2017). Fourier transform and particle swarm optimization based modified LQR algorithm for mitigation of vibrations using magnetorheological dampers. *Smart Materials and Structures*, 26: 115013.

[36] Kumar, G., Kumar, A., Jakka, R. S. An adaptive LQR controller based on PSO and maximum predominant frequency approach for semi-active control scheme using MR damper. *Mechanics & Industry*, 19: 109.

[37] Elliott, S. J. (2002). Signal processing for active control. *Noise Control Engineering Journal*, 50(4): 145–145.